A Location-based MAC Scheme for Random Wireless Network

Xinchen Zhang and Martin Haenggi
Dept. of EE, Univ. of Notre Dame
Notre Dame, IN 46556, USA

***Abstract*—This paper proposes a location-based MAC (LMAC) scheme for wireless networks with randomly placed nodes. This scheme regulates channel access by sharing local location information among transmitters. A lattice approximation approach is used to derive upper and lower bound for the success probability for a typical transmission attempt. Numerical results show that with the node density and link distance fixed, the optimal LMAC provides a much higher density of successful transmissions than CSMA and ALOHA.**

I. Introduction

In wireless networks, different users try to access the same medium. Thus, contention becomes a limiting factor of the MAC layer performance, and managing spatial reuse is a critical issue. The spatial reuse problem gets even more interesting in mobile wireless networks, where off-line scheduling process is impossible due to the network topology dynamics. In such scenarios, CSMA and ALOHA with spatial reuse are intensively investigated (e.g. [1]). The former has been accepted in existing standards (e.g. 802.11), while the latter is also of interest due to its simplicity.

The location-based MAC (LMAC) scheme presented in this paper achieves spatial reuse by sharing location information among nearby users. LMAC is especially suitable for mobile networks, where fairness is inherently achieved. For fixed wireless networks, some modifications need to be introduced to ensure fair medium access. Similar MAC schemes that explore the use of the location information at each user can be found in [2]–[5], where the scheme in [2] is the closest to our scheme in the sense of focusing on spatial reuse with a single channel. However, [2] focuses on information propagation speed, whereas this paper analyzes the spatial throughput in the context of point-to-point communication. Moreover, [2] considers only the 1D case, while this paper deals with the 2D scenario.

The scheduling in LMAC is based on the two criteria[1]:

- A node can transmit only when it is within one of the transmission areas (TAs).
- If there are multiple potential transmitters inside the same TA, only the one closest to the center of this TA transmits.

All the TAs are centered at the vertices on a square lattice $\mathbb{L}$. We use $d_{\mathbb{L}}$ to denote the distance between two nearest vertices on the lattice $\mathbb{L}$. We will consider two kinds of TA shapes: the circular TA and the square TA. For the circular TA, we use r_g to denote the radius of the TA; for the square TA, we assume each side of the TA is $2r_g$. Fig. 1 shows a "snapshot" of a random wireless network using the LMAC scheme.

[1]These two criteria are only principles. There are many ways to implement it. For example, each potential transmitter can set a timer according to its distance to the TA center. The node whose timer expires first broadcasts a signal to declare channel access.

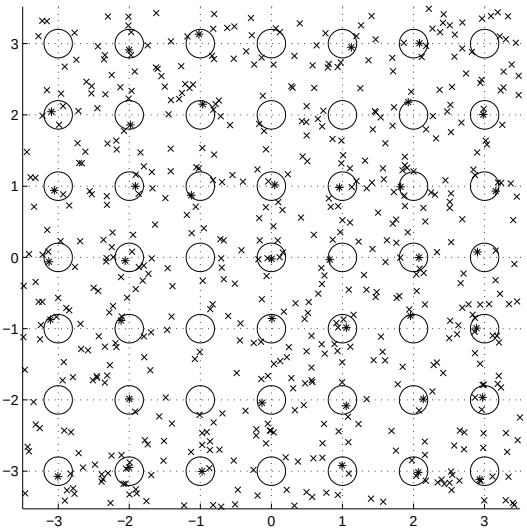

Fig. 1: An example for LMAC, with transmitters distributed as Poisson point process (PPP) and $\lambda = 12$. The TAs are circular areas centered on lattices, $d_{\mathbb{L}} = 1$ and $r_g = 0.2$. All markers indicates a potential transmitter, among which stars are those who are transmitting.

II. System Model and Metrics

A. Network and Transmission Model

We consider a wireless network on the plane $\mathbb{R}^2$, where the potential transmitters are distributed according to homogeneous Poisson point process (PPP) with intensity λ. Each potential transmitter is associated with a dedicated receiver which is located at distance R from the transmitter. This network model is frequently referred to as the Poisson bipolar model in the literature [7].

We assume that each potential transmitter is backlogged and thus transmits whenever it is scheduled to transmit. All the nodes in the network share the same unit bandwidth and transmit at unit power.

B. Reception Model

We shall consider a Rayleigh fading case. The large-scale path loss is r^{α} over distance r. The analysis will be based on the signal to interference ratio (SIR) and outage probability with SIR threshold θ. Suppose there is a transmitter at y and

a receiver at z, where $y, z \in \mathbb{R}^2$. The transmission attempt from y to z is successful, iff

$$\text{SIR}(y,z) \triangleq \frac{H\|y-z\|^{-\alpha}}{\sum_{X\in\Phi_t} H_X\|X-z\|^{-\alpha}} \geq \theta, \qquad (1)$$

where Φ_t is the point process of all other concurrent transmitting nodes; H and H_X represent the fading for the desired transmitter and interferers and are temporally and spatially iid.

C. Performance Metric

The spatial throughput is a widely accepted metric for spatial reuse in wireless networks. It is defined as the mean number of successful transmission per unit area, i.e.,

$$T_s = \lambda_t p_s(\lambda_t, R),$$

where $\lambda_t \leq \lambda$ is the mean number of transmitting nodes per unit area; $p_s(\lambda_t, R)$ is the success probability of a typical transmission attempt.

Note that T_s is not directly associated with any fixed λ. As a result, T_s fails to characterize the utilization of each link, i.e. it cannot guarantee the fraction of time in which each link is activated. For example, if we define $\eta = \lambda_t/\lambda$ and let $\bar{T}_s(\lambda) = \max_\eta \eta\lambda p_s(\eta\lambda, R)$, it can be shown that for small enough R, $\arg\max_\lambda \bar{T}_s(\lambda) \to \infty$, which means each link is activated with probability 0! Moreover, in a practical wireless network, the optimal routing strategy always chooses one of the nearby nodes as desired next hop receiver. Thus, it makes sense to choose a smaller R for a larger λ.

Therefore, this paper focuses on the normalized transmission density defined as

$$D_t \triangleq \frac{T_s}{\lambda}\Big|_{R=1/\sqrt{\lambda}}.$$

Note that $1/\sqrt{\lambda}$ is twice the mean distance of the nearest receiver for the typical node in a PPP network of density λ.

Proposition 1. *For any given shape of the TA and reception threshold θ, if the ratio of the TA size to the size of the Voronoi cell is held constant, i.e. $|TA(o)|/d_{\mathbb{L}}^2 = C$, we have*

$$D_t(\lambda, d_{\mathbb{L}}) \equiv D_t\left(k\lambda, \frac{1}{\sqrt{k}}d_{\mathbb{L}}\right), \quad \forall k \in \mathbb{R}^+.$$

This proposition means the following two scalings result in the same change of D_t: 1) fix the lattice and scale λ by a factor of k; 2) fix λ and scale the lattice constant $d_{\mathbb{L}}$ by a factor of $1/\sqrt{k}$. This result holds because we only consider SIR. If noise is considered, such an equivalent scaling statement will not be true. The proof of Proposition 1 is straightforward.

Corollary 1. *Any D_t achievable in the unit square lattice case ($d_{\mathbb{L}} = 1$) is achievable in the unit potential transmitter density case ($\lambda = 1$).*

Corollary 1 enables us to compare any value of D_t achieved in the unit lattice case to the unit potential transmitter density case. The former is our setup, while the latter is often assumed in the analysis of ALOHA and CSMA (e.g. [1]).

III. Lattice Approximation

Due to the randomness in the location of the transmitting nodes, an exact evaluation of the success probability p_s in LMAC is hard. However, the lattice structure of the TAs indicates that we can use a lattice to approximate the location of interferers. In the square lattice case, let us consider the case where exactly one interferer is located right on each vertex of square lattice $\mathbb{L}\backslash\{o\}$, where o is the origin. Let $|A|$ be the size of a TA. Then, each interferer transmits with probability $p = 1 - e^{-\lambda|A|}$ which is the probability that at least one potential transmitter is inside this TA. We define $p_{\mathbb{L}}^z$ to be the success probability of a transmission attempt to a receiver at z, where the subscript $\mathbb{L}$ implies lattice approximation. Here, the position of the transmitter y is not specified but according to our bipolar model it must satisfy $R = \|y - z\|$. Then, we have the following result:

Proposition 2. *If the interferers are located at $\mathbb{L}\backslash\{o\}$, The success probability of a transmission satisfies*

$$\log p_{\mathbb{L}}^z = -\sum_{x\in\mathbb{L}\backslash\{o\}} l(x-z;\alpha,p,s)|_{s=\theta R^\alpha},$$

where $R = \|y-z\|$ and $l(x;\alpha,p,s) \triangleq -\log\left(1 - \frac{ps}{\|x\|^\alpha + s}\right)$.

Proof: For any TA centered at $x \in \mathbb{L}\backslash\{o\}$, the Laplace transform of its interference to the point z is

$$\mathcal{L}_{I_x}(s) = p\frac{\|x-z\|^\alpha}{\|x-z\|^\alpha + s} + 1 - p.$$

Then, the Laplace transform of the interference is simply

$$\mathcal{L}_I(s) = \prod_{x\in\mathbb{L}\backslash\{o\}} \left(p\frac{\|x-z\|^\alpha}{\|x-z\|^\alpha + s} + 1 - p\right).$$

Also, it is well known that for Rayleigh fading case, the success probability can be expressed by the Laplace transform of interference (e.g. [1]). As a result, we have $p_{\mathbb{L}}^z(y) = \mathcal{L}_I(s)|_{s=\theta R^\alpha}$, where $R = \|y-z\|$. ∎

Some properties of $l(x;\alpha,p,s)$ will be explored in the later sections of the paper. For the sake of simplicity, we will use $l'(\cdot)$ to denote $l(\cdot;\alpha,p,s)$ if there is no confusion.

IV. Transmission Area Shape

A natural question in designing the LMAC is that given the size of the transmission area (TA) $|A|$, what is the best shape of TA? Exploring all the possible shapes of size $|A|$ is intimidating, both analytically and numerically. However, an intuitive answer can be obtained if we consider the limiting case of $\lambda \to \infty$, (and thus $p \to 1$). Then

$$p_{\mathbb{L}}^z = \prod_{x\in\mathbb{L}\backslash\{o\}} \left(1 - \frac{s}{\|x-z\|^\alpha + s}\right)\Big|_{s=\theta R^\alpha}.$$

Since for either T_s or D_t, the success probability $p_{\mathbb{L}}$ is the only factor that will be affected by the shape of TA, the optimal shape of a TA of area $|A|$ maximizes

$$p_{\mathbb{L}} = \mathbb{E}_Z[p_{\mathbb{L}}^Z] = \mathbb{E}_Y\left[\mathbb{E}_Z[p_{\mathbb{L}}^Z \mid Y]\right],$$

where X is the position of the desired transmitter.

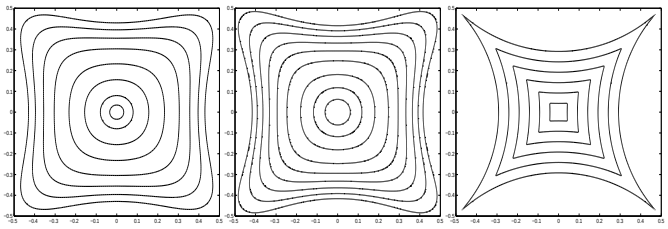

(a) $\alpha = 3$ (b) $\alpha = 4$ (c) $\alpha \to \infty$

Fig. 2: The optimal TA shape in square lattice for different TA sizes. Here, $p = 1$, $R = 0.1$.

If we define the mean success probability for a transmitter at location y as $p_{\mathbb{L}}(y) \triangleq \mathbb{E}_Z\left[p_{\mathbb{L}}^Z \mid Y = y\right]$, where Z is uniformly distributed on the ring of radius R centered at y, we can plot the contour of $p_{\mathbb{L}}(y)$ for all positions within the Voronoi cell of o. For example, Fig. 2a and 2b show the contour for $\alpha = 3$ and 4. In the limiting case $\alpha \to \infty$, it is easily shown that $\log(1 - \frac{s}{x_1^\alpha + s}) = o(\log(1 - \frac{s}{x_2^\alpha + s})), \forall x_1 > x_2 > 0$, which means when $\alpha \to \infty$, it suffices to consider only the interference from the nearest interferer. This fact enables us to analytically characterize $p_{\mathbb{L}}(y)$ for $\alpha \to \infty$ (Fig. 2c).

As expected, Fig. 2 shows $p_{\mathbb{L}}(y)$ becomes smaller as y moves away from o. Let the set of contours in Fig. 2 be a set of TA shapes. Then, the outer contours always have lower $\mathbb{E}[p_{\mathbb{L}}(Y)]$, since Y is distributed in the associated TA. Meanwhile, any other set of shapes cannot have such property. Thus, these contours are the optimal TA shapes.

In principle, we can plot the optimal TA shapes for any set of parameters. Yet, by comparing the contours in Fig. 2, we conclude that for reasonable α either a circle or a square is close to the the optimal TA shape. In fact, numerical results show that in most cases, the performance difference between circular TA and square TA is small. In the following, we will focus on square and circular TA.

V. Bounds on the Success Probability $p_{\mathbb{L}}$

In this section, we bound $p_{\mathbb{L}}$ by evaluating the success probability of a virtual transmitter-receiver pair $(\tilde{y}, \tilde{z})$ while disabling all other potential transmitters in the central TA TA(o). Again, $\|\tilde{y} - \tilde{z}\| = R$. We define this success probability as $\tilde{p}_{\mathbb{L}}^{\tilde{z}}$. Since the pair $(\tilde{y}, \tilde{z})$ is reasonable only if $\tilde{y} \in$ TA(o), we will restrict $\tilde{z} \in$ TA$(o) \oplus b(o, R)$, where $b(o, R)$ is a disk centered at o with radius R and $\oplus$ is the Minkowski addition.

A. Upper bound for $p_{\mathbb{L}}$

First, we try to upper bound the success probability $\tilde{p}_{\mathbb{L}}^{o}$, i.e. $\tilde{z} = o$. Note that this is essentially the best case for $p_{\mathbb{L}}$, because, among all positions within TA$(o) \oplus b(o, R)$, o provides the best spatial separation from interference from other lattice cells.

Before deriving the upper bound, we introduce the following lemma, which states the convex-tail nature of $l(x; \alpha, p, s)$.

Lemma 1. *$l(x; \alpha, p, s)$ is a monotonically decreasing function of $\|x\|$ and is convex for $x > T_c \triangleq \left(\frac{2\alpha s}{\alpha+1}\right)^{\frac{1}{\alpha}}$.*

The proof of Lemma 1 is omitted in this paper. The basic idea is to find the range of x where the second derivative of $l(r; \alpha, p, s)$ is positive.

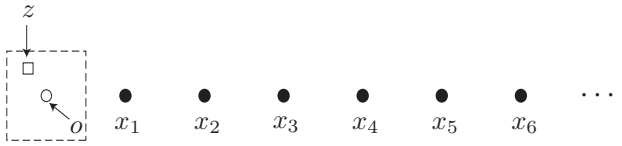

Fig. 3: Interferers on a line.

Meanwhile, it can be easily verified that $l(x; \alpha, p, s) = o(x^{-2})$, as $x \to \infty$ for $\alpha > 2$. Thus, we can use the idea provided in [6] to find a decent upper bound for $\mathcal{L}_I(s)$:

$$\begin{aligned} -\log \mathcal{L}_I(s) &= \sum_{x \in \mathbb{L} \setminus \{o\}} l(x; \alpha, p, s) \\ &> 4 \sum_{k=1}^{K_c - 1} l'(k) + 4 \sum_{k=1}^{K_c - 1} l'(\sqrt{2}k) \\ &\quad + 8 \sum_{k=2}^{K_c - 1} \sum_{i=1}^{k-1} l'(\sqrt{k^2 + i^2}) + 8 \sum_{K_c}^{\infty} k l'(ck), \end{aligned} \tag{2}$$

where $K_c = \lceil T_c \rceil$ and $c \triangleq \frac{\sqrt{2}}{2} + \frac{1}{4}(1 - \log(\sqrt{2} - 1)) \approx 1.1775$. The last term in (2) can be further lower bounded in terms of the Riemann zeta function $\zeta(\cdot)$:

$$\begin{aligned} \sum_{k=K_c}^{\infty} k l'(ck) &= -\sum_{k=K_c}^{\infty} k \log(1 - \frac{ps}{(ck)^\alpha + s}) \\ &> \sum_{k=K_c}^{\infty} \frac{kps}{(ck)^\alpha + s} \\ &> \frac{psK_c^\alpha}{c^\alpha K_c^\alpha + s} \sum_{k=K_c}^{\infty} k^{1-\alpha} \\ &= \frac{psK_c^\alpha}{c^\alpha K_c^\alpha + s} \left(\zeta(\alpha - 1) - \sum_{k=1}^{K_c - 1} k^{1-\alpha} \right). \end{aligned}$$

Consequently, we have a strict lower bound for $-\mathcal{L}_I(s)$ in terms of the Riemann zeta function, and thus an corresponding upper bound for $p_{\mathbb{L}}^o$. Since $p_{\mathbb{L}}^o \geq p_{\mathbb{L}}$, this upper bound is also an strict upper bound for $p_{\mathbb{L}}$.

B. Lower bound for $p_{\mathbb{L}}$

Similarly, using the virtual transmitter-receiver pair argument, we can derive a lower bound of $p_{\mathbb{L}}$. Before doing that, we give some results dealing with intereference from part of the lattice network to an arbitrary receiver position z.

1) Interference from a line of interferers: We first consider the interference from a line of interferers. Fig. 3 shows a simple example of one dimensional interferers, where all the solid dots are the interferers and the desired receiver is assumed to be located at z. Generally, a line of interferers is defined as interferers located at $x_i = ix_1,\ i = 1, 2, 3, \ldots$. In the example in Fig. 3, $x_1 = [1, 0]^T$. For the sake of simplicity, we further assume $\|z\| \leq \|x_i\|,\ \forall i$.

Proposition 3. *$\forall K_B \in \mathbb{Z}^+$, define the two constants $c_1 \triangleq \|z - x_{K_B+1}\| - \|z - x_{K_B}\|,\ b_1 \triangleq \|z - x_{K_B}\| - c_1 K_B$. Then, $\forall K \in \mathbb{Z}^+$, such that $K \geq \max\{T_{c,1} + \frac{1}{2}, K_B\}$:*

$$\sum_{k=K}^{\infty} l'(\|z - x_k\|) \leq \frac{1}{c_1} I_1^\infty(b_1 + c_1(K - \frac{1}{2})),$$

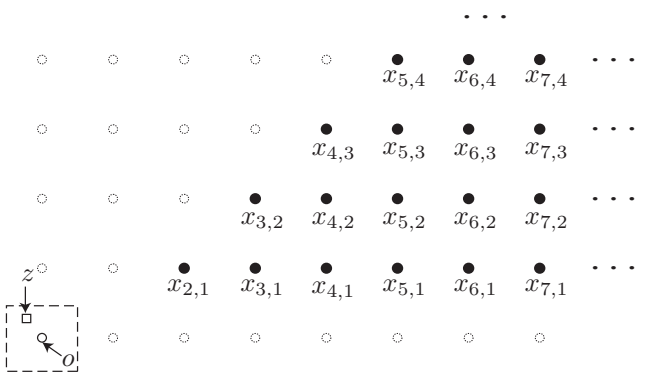

Fig. 4: Interferers in a triangular region.

where $I_1^\infty(x) \triangleq \int_x^\infty l'(t)\mathrm{d}t$.

Proof: Since for any $k \in \mathbb{Z}^+$,

$$\|x_{k+1} - z\| - \|x_k - z\| \leq \|x_{k+2} - z\| - \|x_{k+1} - z\|,$$

we know that for any $k \geq K_B$

$$\|x_k - z\| \geq \|x_{K_B} - z\| + (k - K_B)c_1.$$

By the monotonicity and convexity proved in Lemma 1, we have: for any $k \geq \max\{K_B, T_{c,1} + \frac{1}{2}\}$,

$$l'(\|z - x_k\|) \leq l'(b_1 + c_1 k) \leq \int_{k-\frac{1}{2}}^{k+\frac{1}{2}} l'(b_1 + c_1 x)\mathrm{d}x.$$

Summing this inequality for all $k \geq K \geq \max\{K_B, T_{c,1} + \frac{1}{2}\}$ yields the desired result. ■

Note that $I_1^\infty(x)$ is not in closed form, but it can be expressed by gamma function and hypergeometric function, and thus can be evaluated with arbitrary numerical precision.

2) Interference from a triangular region: Fig. 4 shows an example of interferers in a triangular region, where all the solid dots are interferers, all the dotted circles in the figure are only for reference. Generally, we define $x_{k,i} = kx_{k0} + ix_{i0}$ as the intereferers in a triangular region, where $k = 2, 3, \ldots$, $1 \leq i \leq k-1$, and $x_{k0}, x_{i0} \in \mathbb{R}^2$ are orthogonal constant vectors. In the previous example, $x_{k0} = [1, 0]^T$, $x_{i0} = [0, 1]^T$. Again, we assume $\|z\| \leq \|x_{k,i}\|,\ \forall k, i$.

Lemma 2. $\forall b_2, c_2 \in \mathbb{R}^+$, $f(x) \triangleq (x-1)l'(b_2 + c_2 x)$ *is convex for* $x \geq T_{c,2} \triangleq \max\{3 + \frac{6b_2}{\alpha c_2}, (6^{\frac{1}{\alpha}} - b_2)/c_2, \frac{1}{c_2}\left(\frac{6b_2 s}{\alpha c_2}\right)^{\frac{1}{\alpha}} - \frac{b_2}{c_2}\}$.

We omit the proof of Lemma 2 which is simply bounding the second derivative of $(x-1)l'(b_2 + c_2 x)$.

Proposition 4. $\forall K_B \in \mathbb{Z}^+$, *define the two constants* $c_2 \triangleq \|x_{K_B+1,1} - z\| - \|x_{K_B,1} - z\|$, $b_2 \triangleq \|x_{K_B,1} - z\| - c_2$. *Then,* $\forall K \in \mathbb{Z}^+$, *such that* $K \geq \max\{K_B, T_{c,1}, T_{c,2} + \frac{1}{2}\}$:

$$\sum_{k=K}^{\infty}\sum_{i=1}^{k-1} l'(\|z - x_{k,i}\|) < \frac{1}{c_2^2} I_2^\infty\left(b_2 + c_2(K - \frac{1}{2})\right) - \frac{b_2 + c_2}{c_2^2} I_1^\infty\left(b_2 + c_2(K - \frac{1}{2})\right),$$

where $I_1^\infty(x) \triangleq \int_x^\infty l'(t)\mathrm{d}t$ *and* $I_2^\infty(x) \triangleq \int_x^\infty t l'(t)\mathrm{d}t$.

Proof: By the definition of $x_{k,i}$, it is obvious that $\|x_{k,i} - z\| \geq \|x_{k,1} - z\|, \forall i \geq 1$. Combining this with the monotonicity of $l'(x)$, we have $\sum_{i=1}^{k-1} l'(\|x_{k,i} - z\|) \leq (k-1)l'(\|x_{k,1} - z\|)$. Similar to the argument we made in Proposition 3, we have

$$\|x_{x,1} - z\| \geq \|x_{K_B,1} - z\| + (k - K_B)c, \forall k \geq K_B, k \in \mathbb{Z}^+.$$

Then, using the monotonicity of $l'(x)$ proved in Lemma 1 as well as the convexity of $(x-1)l'(b_2 + c_2 x)$ proved in Lemma 2, we have: for all $k \geq \max\{K_B, T_{c,1}, T_{c,2} + \frac{1}{2}\}$,

$$l'(\|x_{k,1} - z\|) \leq \int_{k-\frac{1}{2}}^{k+\frac{1}{2}} (x-1)l'(b_2 + c_2 x)\mathrm{d}x.$$

Summing over all $k \geq K \geq \max\{K_B, T_{c,1}, T_{c,2} + \frac{1}{2}\}$ yields the desired result. ■

Note that, similar to $I_1^\infty(x)$, $I_2^\infty(x)$ can be expressed in terms of gamma function and hypergeometric function.

Because the whole lattice network (except for the central point o) can be divided into eight triangular regions and eight interferer lines, the above two propositions can provide an upper bound for $\sum_{x \in \mathbb{L} \setminus \{o\}} l'(\|x - z\|)$ and thus a lower bound for $\tilde{p}_{\mathbb{L}}^z$. Since $\min_{z \in \mathrm{TA}(o) \oplus b(o,R)} \tilde{p}_{\mathbb{L}}^z \leq p_{\mathbb{L}}$, if we can find the worst realization of z, we have a lower bound for $p_{\mathbb{L}}$. This worst case z depends on the TA shape we choose, but we know it must be located on the boundary of $\mathrm{TA}(o) \oplus b(o, R)$.

Specifically, simulation results show that for circular TAs of radius r_g, we have

$$\arg \min_{z \in \mathrm{TA}(o) \oplus b(o,R)} \tilde{p}_{\mathbb{L}}^z = \arg \min_{z \in \{z_1, z_2\}} \tilde{p}_{\mathbb{L}}^z, \tag{3}$$

where $z_1 = [0, R + r_g]^T$, $z_2 = [\frac{1}{\sqrt{2}}(R + r_g), \frac{1}{\sqrt{2}}(R + r_g)]^T$. For square TA with each side of $2r_g$, (3) still holds but with $z_1 = [0, R + r_g]^T$, $z_2 = [R + \frac{1}{\sqrt{2}} r_g, R + \frac{1}{\sqrt{2}} r_g]^T$.

C. Numerical Example

Fig. 5 plots the transmission density D_t as a function of λ for different TA sizes. Here, the TA shape are chosen to be square. By the figures, we can see our upper and lower bound approximates the p_s of LMAC pretty well when the TA is small (for $r_g = 0.1$ and $r_g = 0.2$). As expected, the lower bound becomes looser when $r_g = 0.4$, where the worst case effect is mitigated by choosing the transmitter nearest to the TA center.

VI. Comparison with ALOHA and CSMA

The performance of ALOHA is analytically tractable [1]. However, the exact performance of CSMA is still generally not well characterized. Almost all the analysis for CSMA involves certain level of approximation. In the following two subsections, we will base our comparison to CSMA on two analytical results which are presented in [1] and [7] respectively.

A. Comparison 1: Matern Process Approximation

Fig. 6 uses the upper and lower bound of p_s derived above to characterize the normalized transmission density for LMAC and compares it with CSMA and ALOHA schemes. The lower bound of LMAC is calculated in a max-min fashion, i.e. it is the maximum of the lower bound of D_t among all choices of λ and r_g. The upper bound in the figure is the upper

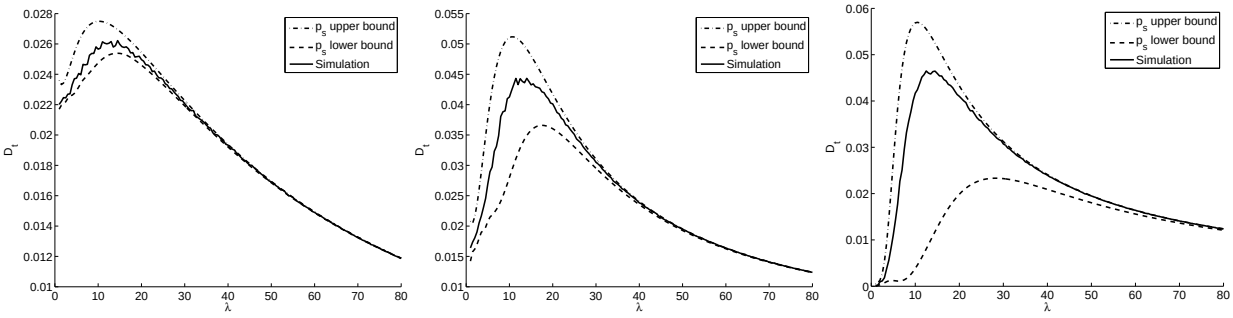

(a) $r_g = 0.1$ (b) $r_g = 0.2$ (c) $r_g = 0.4$

Fig. 5: Calculated Transmission Density using 1) $p_{\mathbb{L}}$ upper bound, 2) $p_{\mathbb{L}}$ lower bound, 3) simulation results. $\alpha = 4$, $R = 1$, $\lambda = 1$, $\theta = 10$.

bound of D_t when λ and r_g are chosen as the value that maximizes the lower bound. The performance of CSMA and ALOHA are cited from [1], where the authors approximate concurrent transmitter in CSMA to form a Matern hard core process. Its density is $\lambda_{R_{cs}} = (1 - e^{-\pi\lambda R_{cs}^2})/(\pi R_{cs}^2)$, where $R_{cs} = \frac{2}{\sqrt{3}} R \left(2\theta\zeta(\alpha-1)\right)^{1/\alpha}$ is the corresponding carrier sensing range. To get normalized transmission density, we simply apply $\lambda = 1$ and $R = 1$ to the functions above.

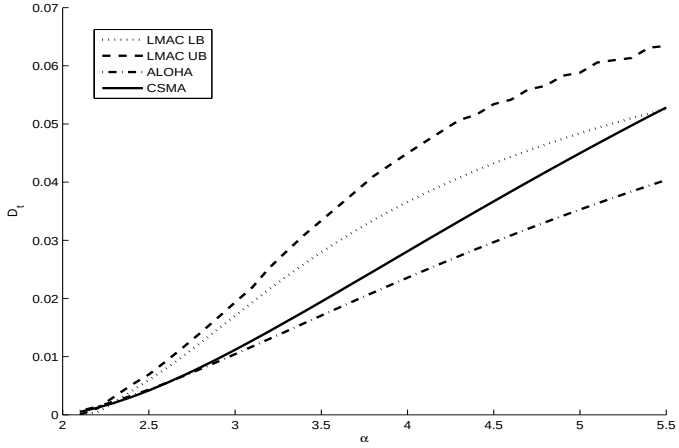

Fig. 6: Comparison of normalized transmission density among different MAC schemes, where $\theta = 10$. Here, the CSMA and ALOHA performance are cited from [1]. The performance of LMAC is evaluated by the analytical lower bound.

Fig. 6 shows for (at least) $2.5 \leq \alpha \leq 5.5$ even the lower bound of the LMAC outperforms both CSMA and ALOHA.

B. Comparison 2: Poisson Process Approximation

Table I compares the normalized transmission density of LMAC with ALOHA and CSMA. Here, the results about CSMA are obtained by approximating the transmitting point process Φ_t to be a Matern point process then approximating it by an inhomogeneous Poisson point process [7]. In such a framework, when $R = 1$, the transmitting success probability of a typical transmittion attempt is

$$p_s^{\text{CS}}(P_o) \approx \exp\left(-\lambda \int_{\mathbb{R}^+} \int_0^{2\pi} \frac{\tau h(\tau, P_o)}{1 + \frac{(\tau^2+1-2\tau\cos\phi)^{\alpha/2}}{\theta}} \mathrm{d}\phi \mathrm{d}\tau\right),$$

where P_o is the detection threshold for carrier sensing and $h(r, P_o)$ is the probability of two node, at distance r, access the medium at the same time. $h(r, P_o)$ can be written in the form of an integral over the $\mathbb{R}^2$ plane. Then, the normalized transmission density is $pp_s^{\text{CS}}(P_o)$, where $p = (1 - e^{\bar{N}})/\bar{N}$ is the transmitting probability of each node and $\bar{N} = \frac{2\pi\Gamma(2/\alpha)}{\alpha P_o^{2/\alpha}}$. The value shown in Table I is $\max_{P_o} pp_s^{\text{CS}}(P_o)$.

TABLE I: Performance Comparison of Different MAC Schemes in 2D case: fix $\alpha = 4$, $R = 1$, $\lambda = 1$, $\theta = 10$.

Scheme	$\max D_t$	D	p_s
LMAC	0.047	0.068	0.69
CSMA	0.037	0.072	0.52
ALOHA	0.024	0.064	0.38

Table I shows that: in terms of normalized transmission density, LMAC outperforms CSMA by 27% and ALOHA by 96%. It also demonstrates that LMAC has better transmission success probability than CSMA or ALOHA, which can potentially reduce the local delay [8] and the energy spent on unsuccessful transmissions.

ACKNOWLEDGMENT

The partial support of NSF (grants CCF 728763) and the DARPA/IPTO IT-MANET program (grant W911NF-07-1-0028) is gratefully acknowledged.

REFERENCES

[1] F. Baccelli, B. Blaszczyszyn, and P. Muhlethaler, "An Aloha protocol for multihop mobile wireless networks," *IEEE Trans. Inf. Theory*, vol. 52, no. 2, pp. 421-436, Feb. 2006.

[2] N.Wen and R. Berry, Location-based MAC protocols for mobile wireless networks," *2007 Information Theory and Applications Workshop (ITA)*, San Diego, CA, USA, 2007.

[3] S. Katragadda, G. Murthy, R. Rao, M. Kumar, and R. Sachin,"A decentralized location-based channel acce protocol for inter-vehicle communication," *Proc. of IEEE VTC 2003- Spring*, April 2003.

[4] S. V. Bana and P. Varaiya, "Space division multiple access (SDM for robust ad hoc vehicle communication networks," *Proc. of IEEE Intelligent Transportation Systems*, Oakland, CA, USA, Aug. 2001.

[5] J. J. Blum and A. Eskandarian, "Adaptive space division multiplexing: an improved link layer protocol for inter-vehicle communications," *Proc. of IEEE Intelligent Transportation Systems*, Sept. 2005.

[6] M. Haenggi, "Interference in Lattice Networks", http://arxiv.org/abs/1004.0027.

[7] F. Baccelli and B. Blaszczyszyn, *Stochastic Geometry and Wireless Networks.* Foundations and Trends in Networking, NOW, 2009.

[8] M. Haenggi, "Local Delay in Static and Highly Mobile Poisson Networks with ALOHA," *2010 IEEE International Conference on Communications (ICC'10)*, May 2010.